Supporting Information

Computational Screening of Defective BC_3-Supported Single-Atom Catalysts for Electrochemical CO_2 Reduction

Renyi Li[1], Caimu Wang[1], Yaozhong Liu[1], Chengxiang Suo[1], Danyang Zhang[1], Jiao Zhang[1], Wei Guo*[,1,2]

[1] *Centre for Quantum Physics, Key Laboratory of Advanced Optoelectronic Quantum Architecture and Measurement (MOE), School of Physics, Beijing Institute of Technology, Beijing 100081, China*

[2] *Frontiers Science Center for High Energy Material (MOE), Beijing Institute of Technology, Beijing 100081, China*

Note:

The ΔG(*OCHO) and ΔG(*COOH) are the free energy changes of the two intermediates after the first hydrogenation step of eCO_2RR (* denotes the catalyst):

$$* + CO_2 + H^+ + e^- \rightarrow *OCHO$$

$$* + CO_2 + H^+ + e^- \rightarrow *COOH$$

which can be obtained by the definition:

$$\Delta G(*OCHO) = G(*OCHO) - G(*) - G(CO_2) - G(H^+ + e^-)$$

$$\Delta G(*COOH) = G(*COOH) - G(*) - G(CO_2) - G(H^+ + e^-)$$

where G(*OCHO), G(*COOH) and G(*) are the free energies of *OCHO, *COOH and catalyst. G(CO_2) is the free energy of a CO_2 in gas phase. G($H^+ + e^-$) is the free energy of the proton-electron pair, which can be calculated by setting the reference potential to the potential of the standard hydrogen electrode[1]:

$$H^+ + e^- \rightarrow 1/2H_2$$

ΔG of this reaction is expressed as below:

$$\Delta G = 1/2G(H_2) - G(H^+ + e^-),$$

when this reaction is in equilibrium and ΔG is equal to 0, i.e., G($H^+ + e^-$) is equal to half the free energy of H_2. Similarly, ΔG(*H) can be calculated by the formula:

$$\Delta G(*H) = G(*H) - G(*) - 1/2G(H_2),$$

where G(*H) is the free energy of H adsorbed on catalyst. The comparison of ΔG(*OCHO or *COOH) and ΔG(*H) enables the estimation of the selectivity between eCO_2RR and HER[2].

Table S1 Structural parameters and band gap of BC_3 monolayer.

	Lattice constant (Å)	$l_{C\text{-}C}$ (Å)	$l_{C\text{-}B}$ (Å)	Band gap (eV)
This work (PBE)	5.17	1.42	1.56	0.63
Theor. (PBE)[3]	5.17	1.42	1.56	0.65
Theor. (PBE)[4]	5.17	1.42	1.56	0.61
Exp.[5]	5.20±0.2	1.42	1.55	/

Table S2 The values of U – J parameters for PBE+U calculations[6,7].

TM	**Sc**	**Ti**	**V**	**Cr**	**Mn**	**Fe**	**Co**	**Ni**	**Cu**	**Zn**
U – J	2.11	2.58	2.72	2.79	3.06	3.29	3.42	3.40	3.87	4.12

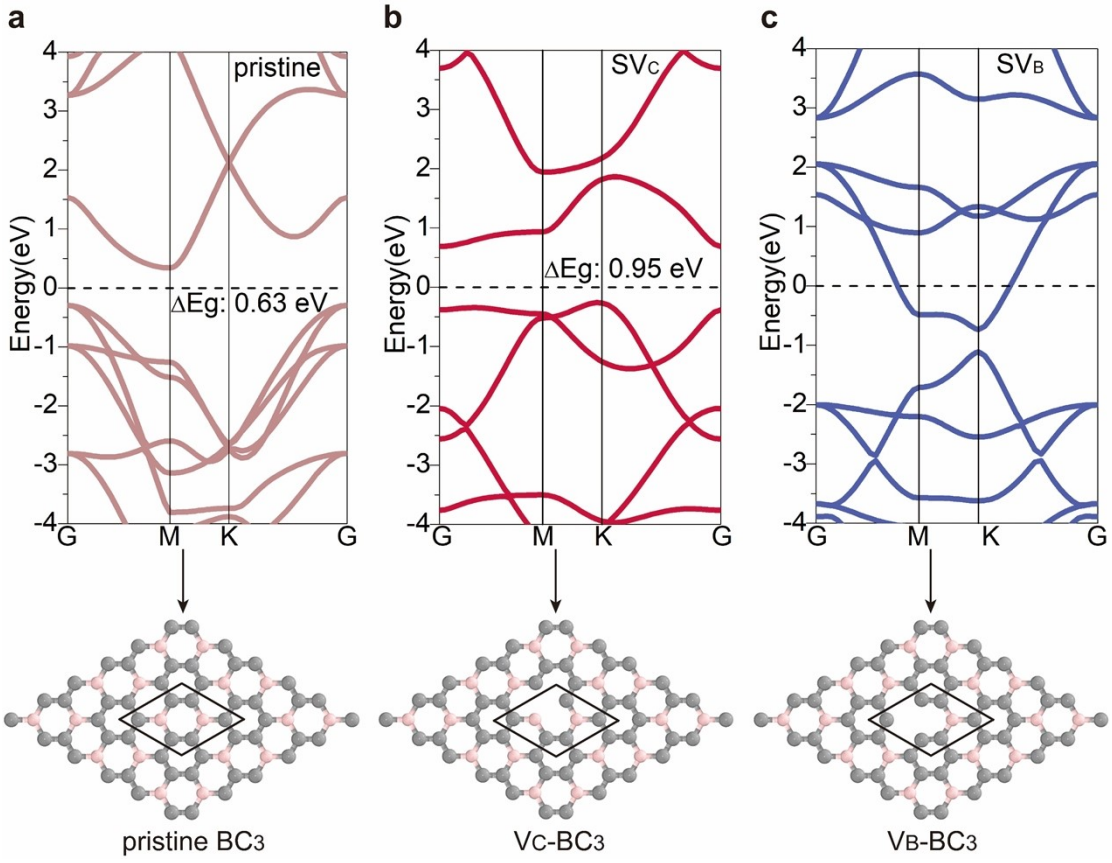

Figure S1. Band structures of **(a)** pristine BC_3, **(b)** V_C-BC_3 and **(c)** V_B-BC_3. The atomic structures

are shown below. The solid lines represent the lattice of the unit cell. The band structures are calculated using the unit cells of pristine BC_3 and defective BC_3.

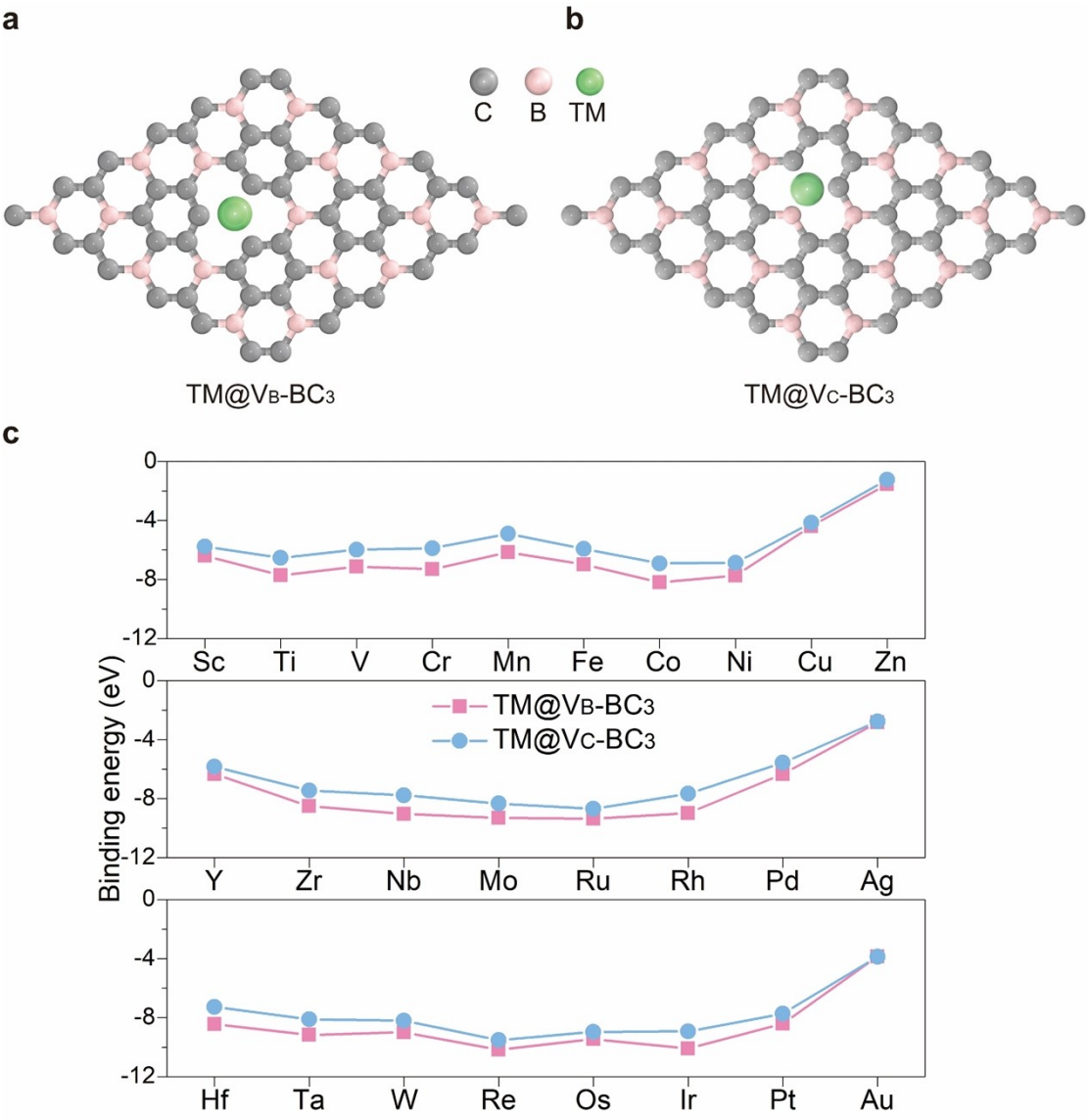

Figure S2. Structural models of **(a)** TM@V_B-BC_3 and **(b)** TM@V_C-BC_3. (**c**) Binding energy of TM SAs anchored on V_B-BC_3 and V_C-BC_3.

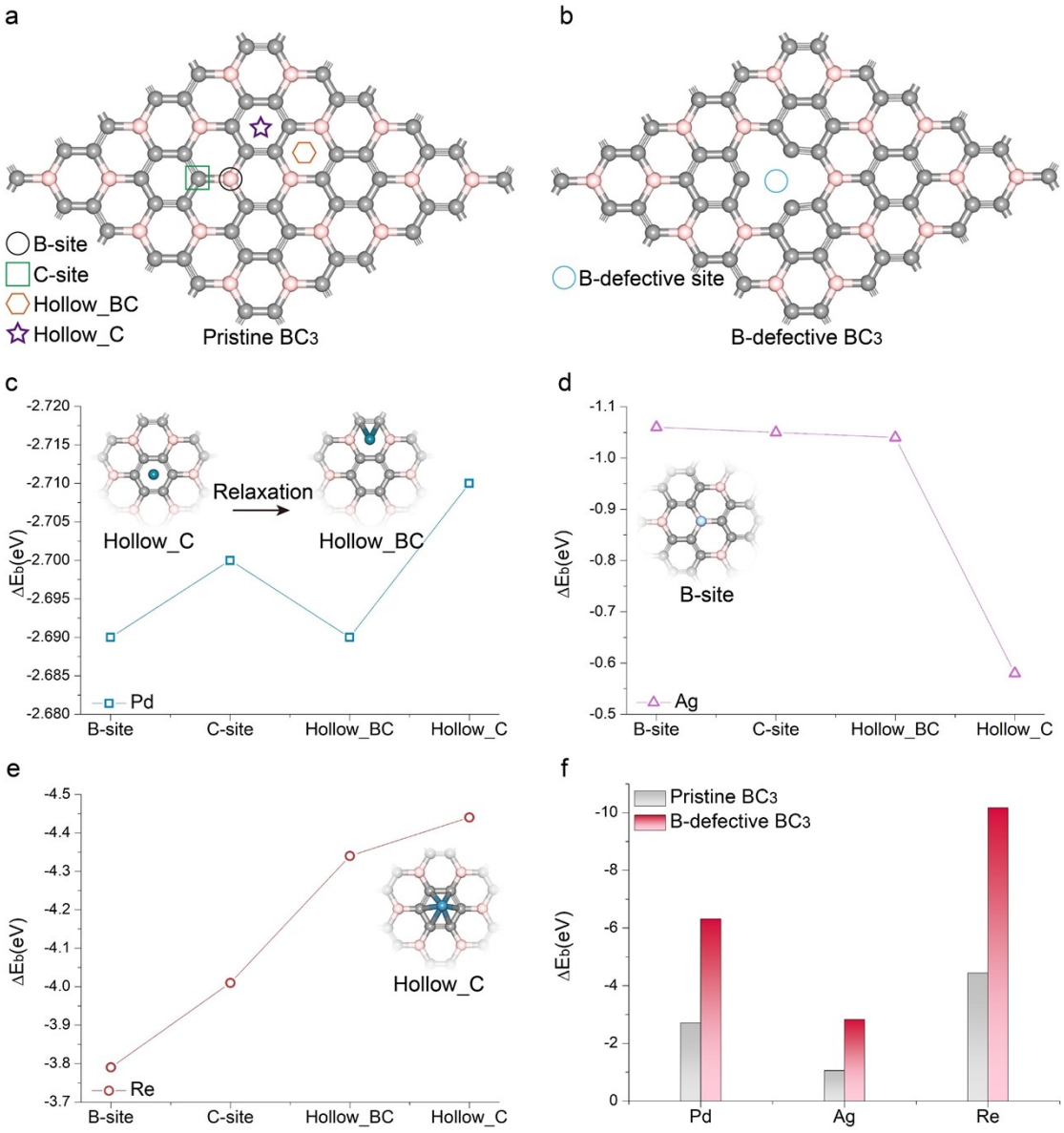

Figure S3. Anchoring sites of TM SAs on **(a)** pristine BC_3 and (**b**) B-defective BC_3. Binding energy (ΔE_b) of **(c)** Pd, **(d)** Ag and **(e)** Re on pristine BC_3. **(f)** ΔE_b of TM SAs on pristine BC_3 and B-defective BC_3.

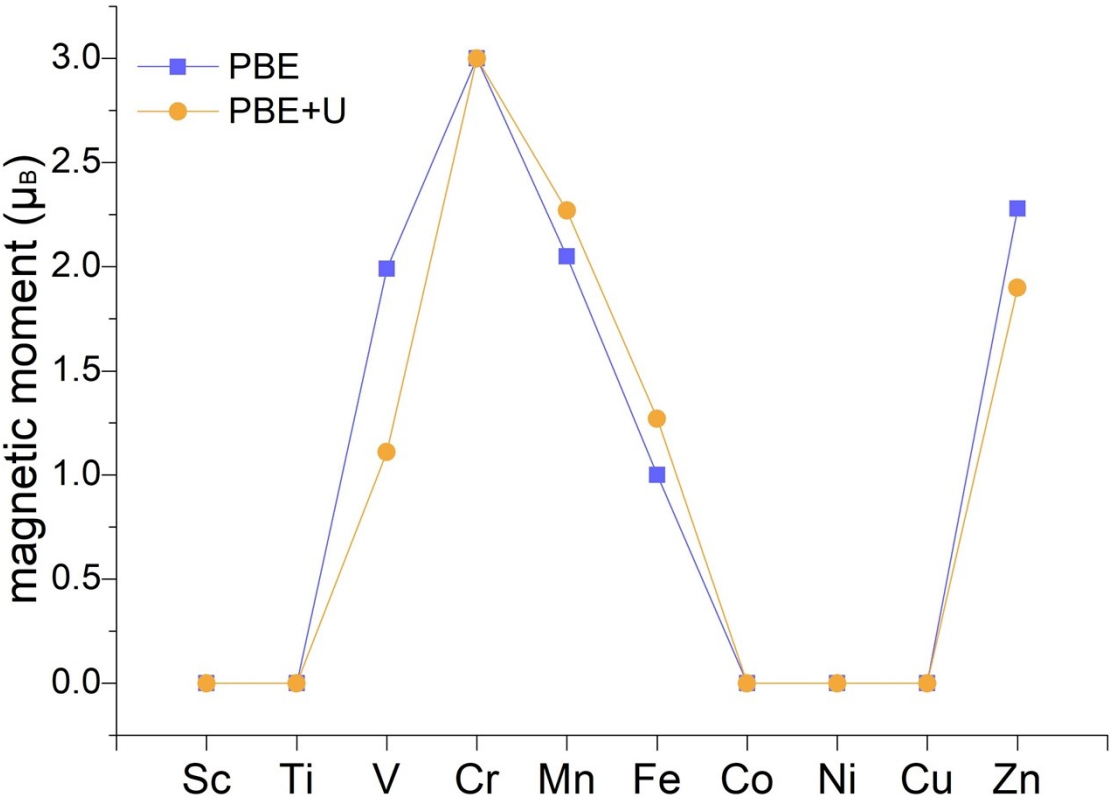

Figure S4. Magnetic moment (μ_B) of 3d TM SAs in TM@ BC_3 at PBE level and PBE+U level.

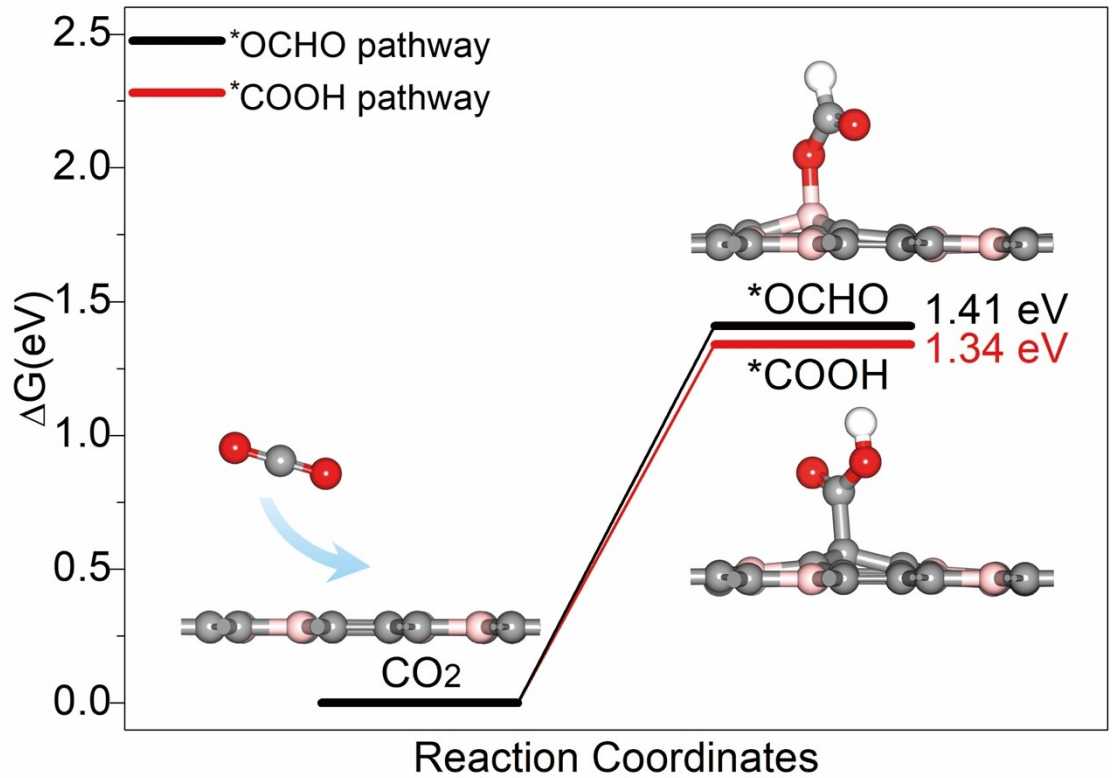

Figure S5. Free energy diagram of eCO_2RR to *OCHO and *COOH intermediates on pristine BC_3.

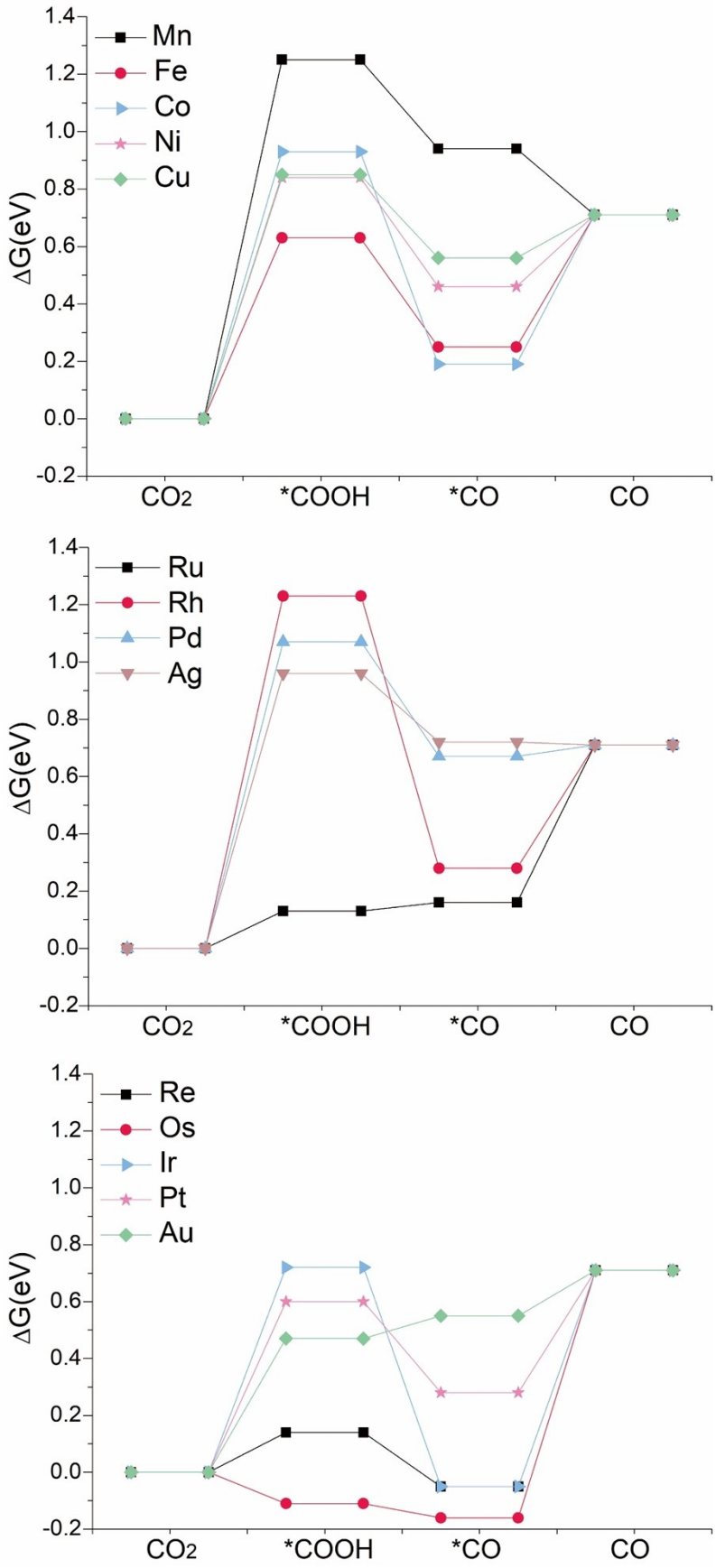

Figure S6. Free energy diagrams of eCO_2RR to CO on $TM@BC_3$.

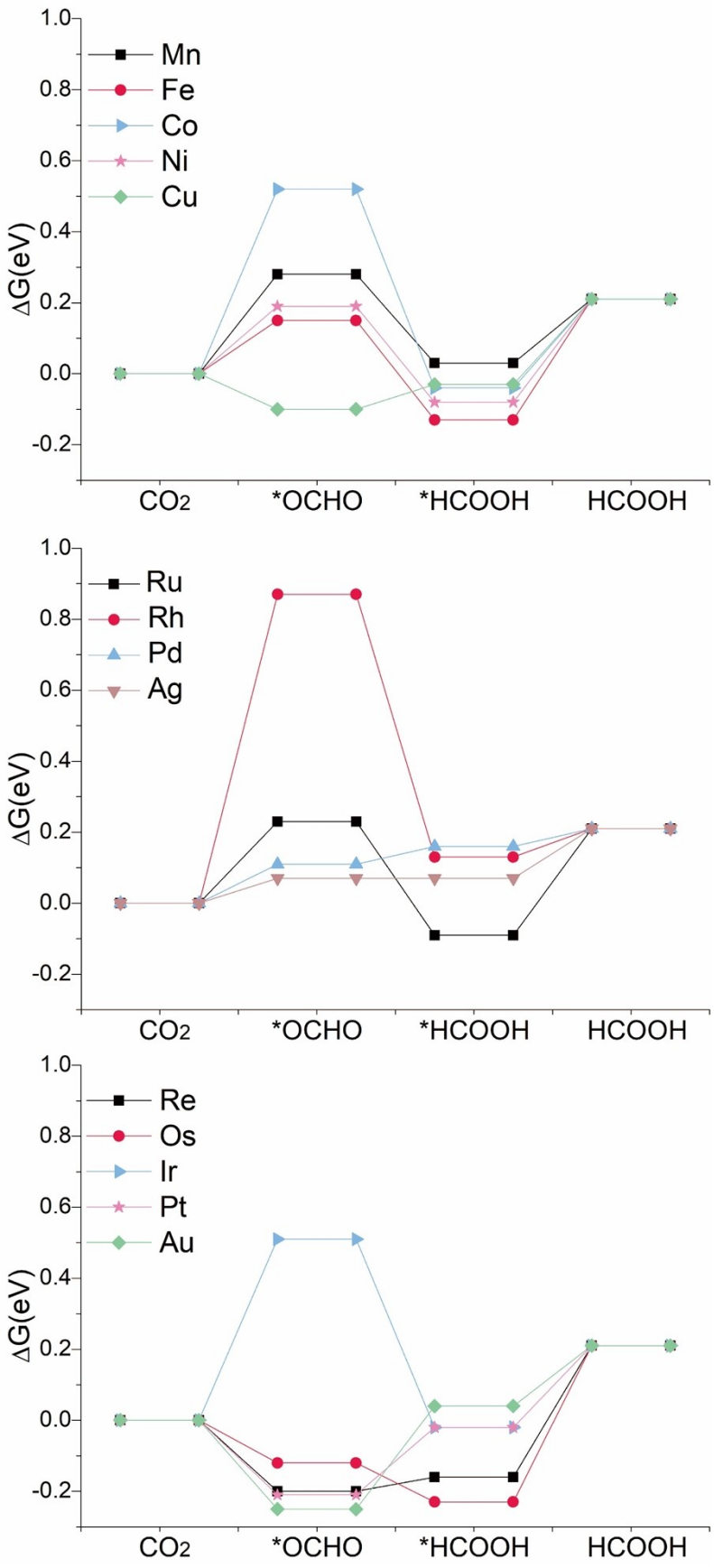

Figure S7. Free energy diagrams of eCO_2RR to HCOOH on $TM@BC_3$.

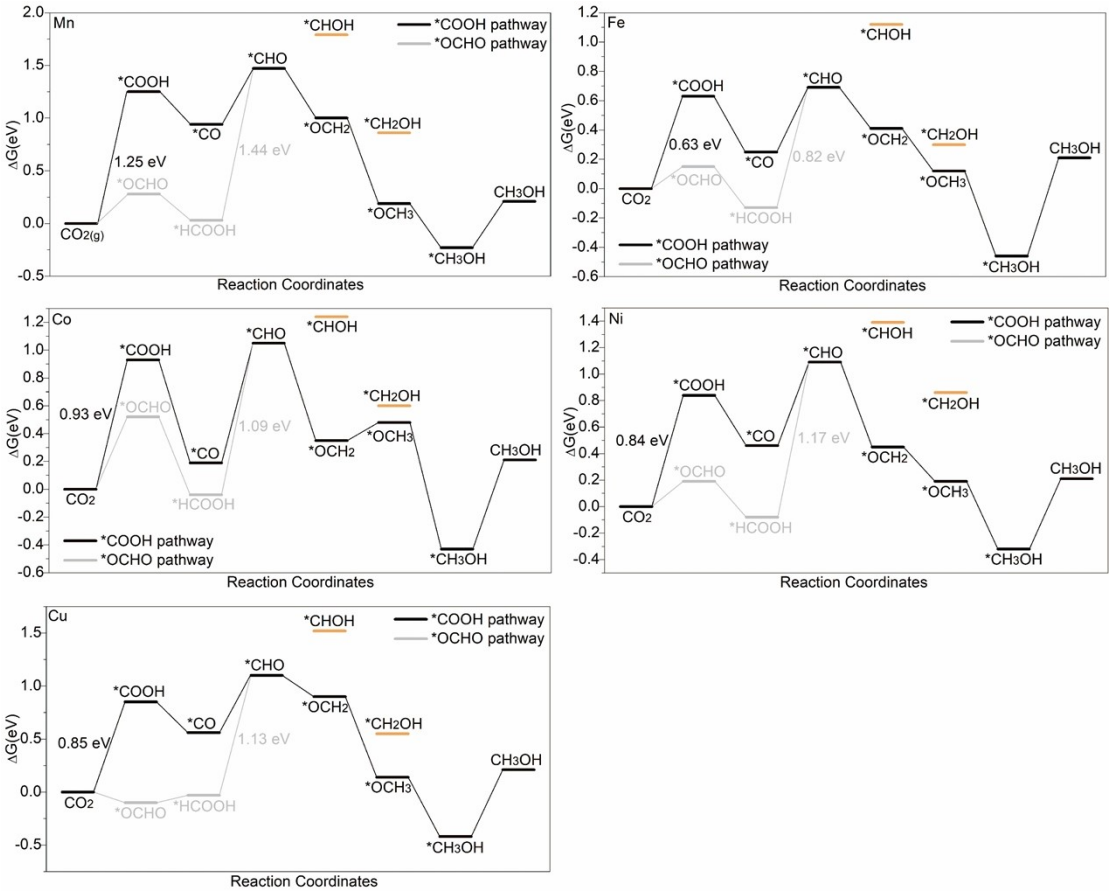

Figure S8. Free energy diagrams of eCO_2RR to CH_3OH on $TM@BC_3$.

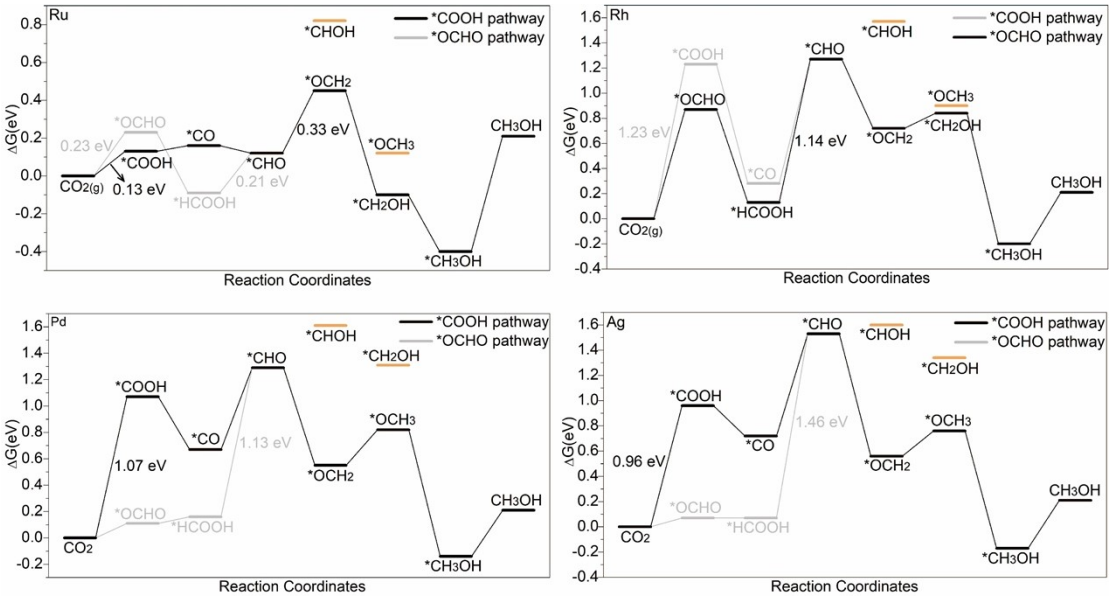

Figure S9. Free energy diagrams of eCO_2RR to CH_3OH on $TM@BC_3$.

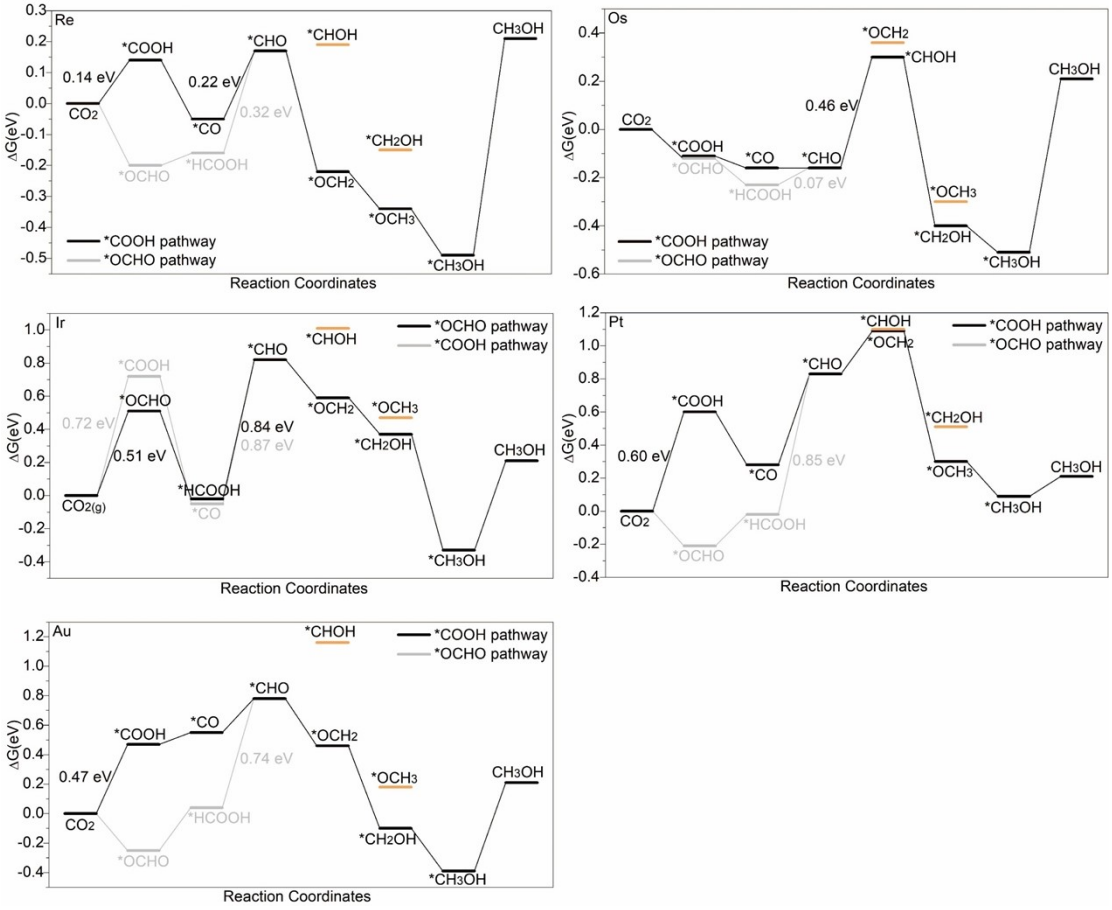

Figure S10. Free energy diagrams of eCO_2RR to CH_3OH on $TM@BC_3$.

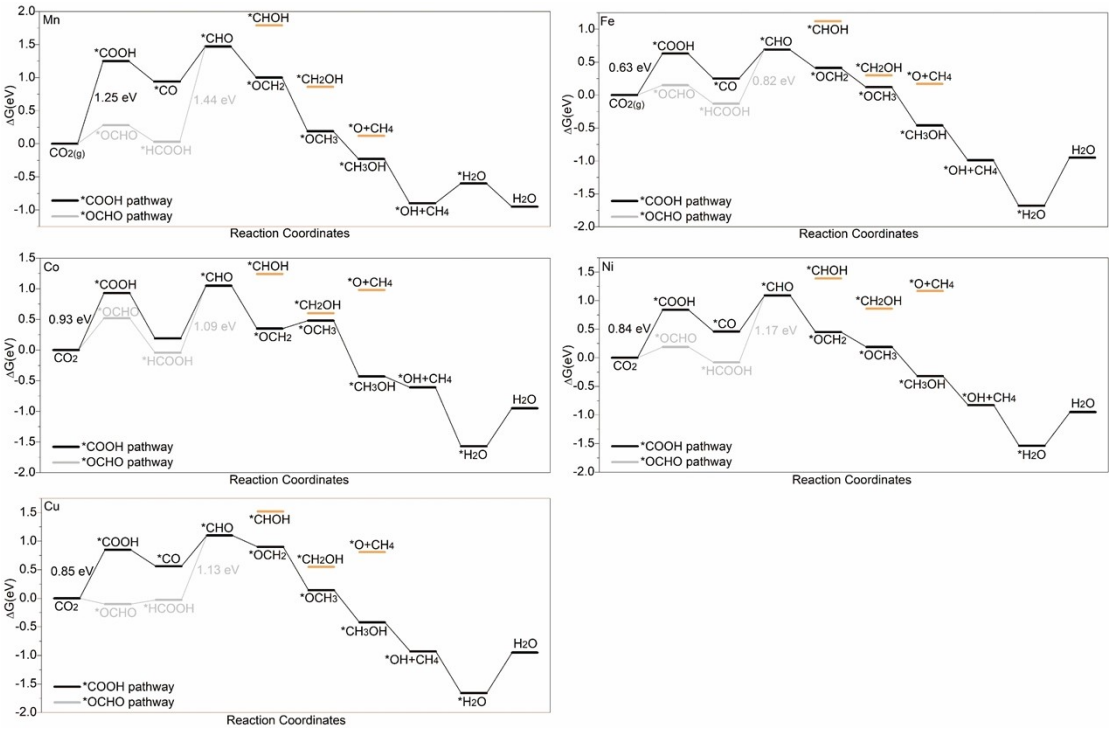

Figure S11. Free energy diagrams of eCO_2RR to CH_4 on $TM@BC_3$.

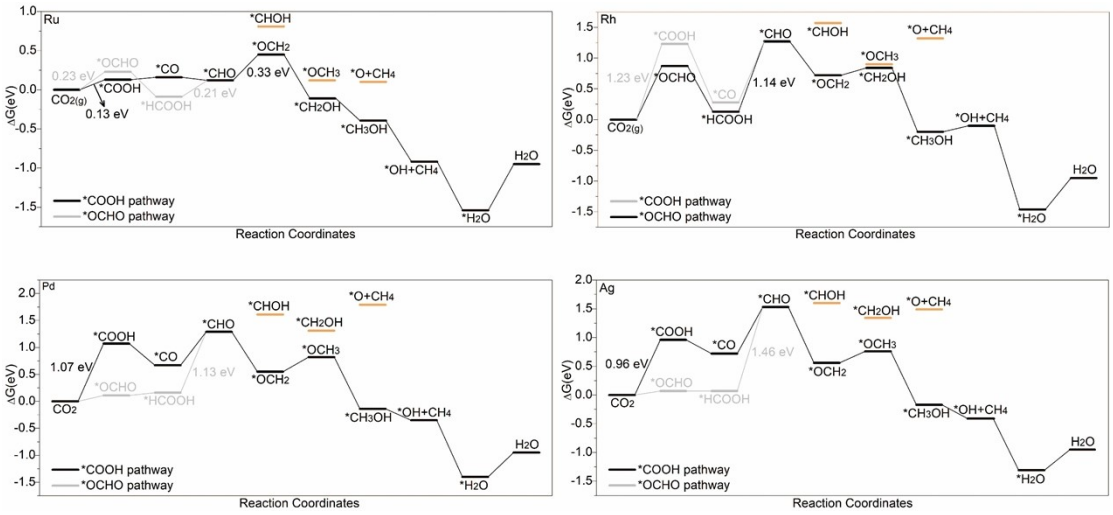

Figure S12. Free energy diagrams of eCO_2RR to CH_4 on $TM@BC_3$.

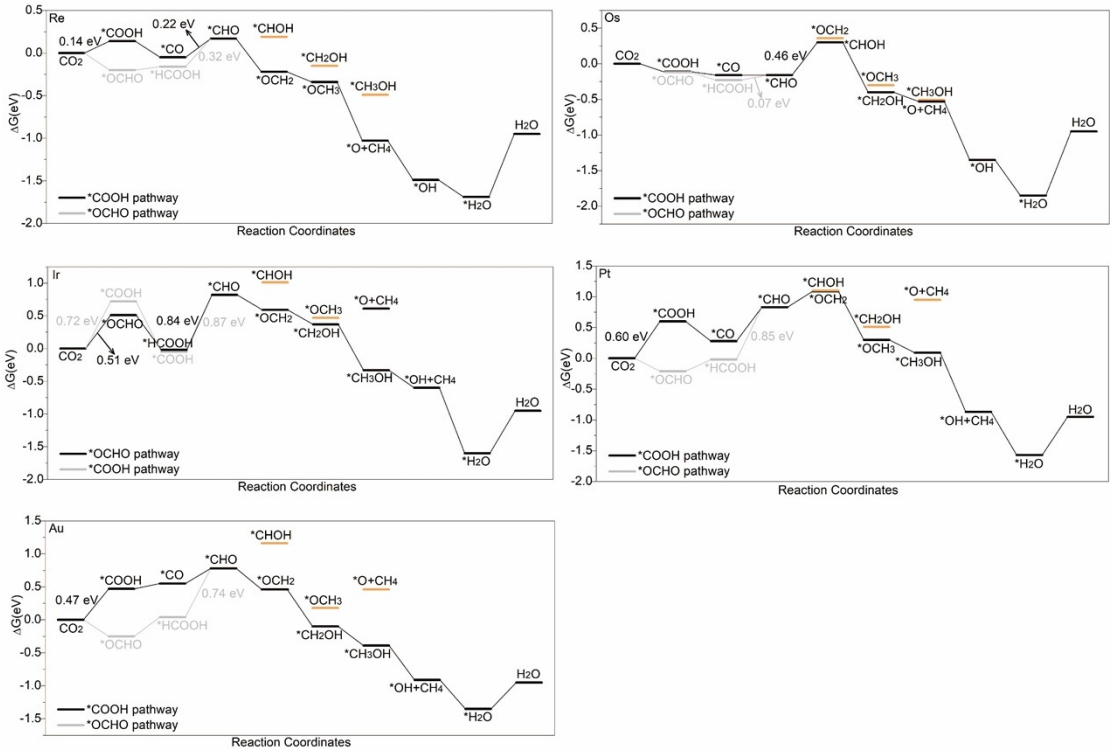

Figure S13. Free energy diagrams of eCO_2RR to CH_4 on $TM@BC_3$.

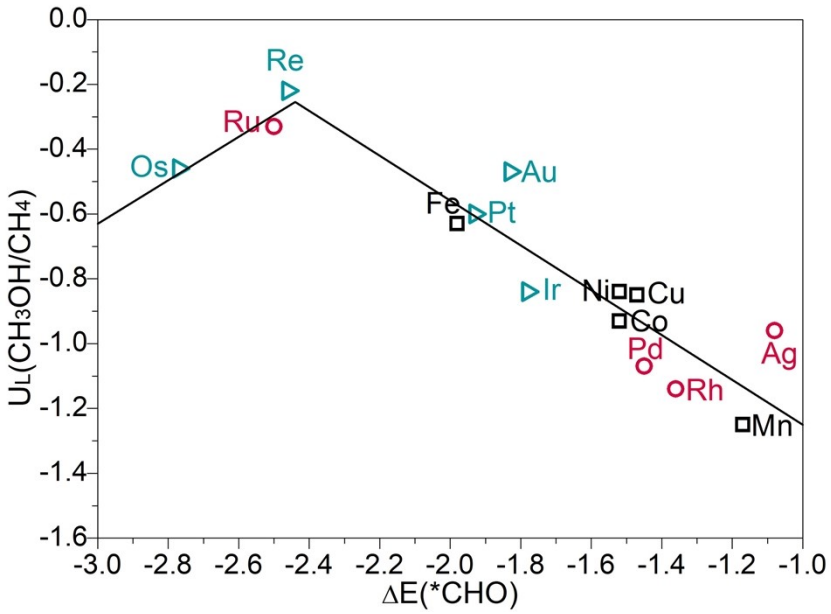

Figure S14. Volcano-shaped relation between the adsorption energy of *CHO and the U_L for CH_3OH and CH_4 production.

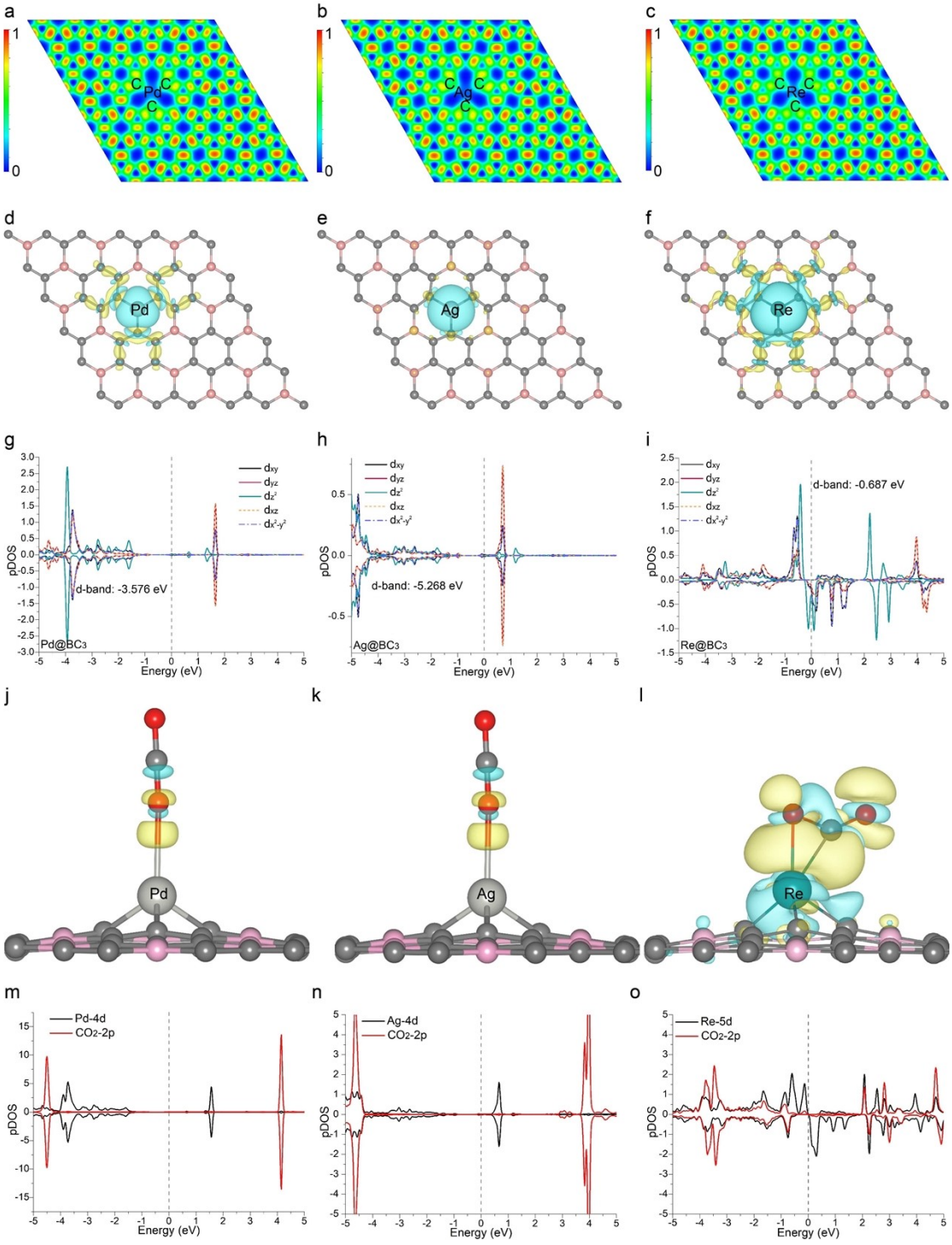

Figure S15. Electronic structures of Pd, Ag and Re@BC_3 SACs and CO_2 adsorption. Electron localization function (ELF) of **(a)** Pd, **(b)** Ag and **(c)** Re@BC_3 SACs**.** Charge density difference (CDD) between **(d)** Pd, **(e)** Ag, **(f)** Re SAs and B-defective BC_3. Projected density of states (pDOS) of **(g)** Pd, **(h)** Ag, and **(i)** Re d sub-orbitals. CDD between CO_2 and **(j)** Pd, **(k)** Ag and **(l)** Re@BC_3 SACs. pDOS of CO_2-2p and **(m)** Pd-4d, **(n)** Ag-4d and **(o)** Re-5d orbitals. Yellow and cyan regions indicate the accumulation and depletion of electron densities at the isosurface value of 0.002 e/Å^3.

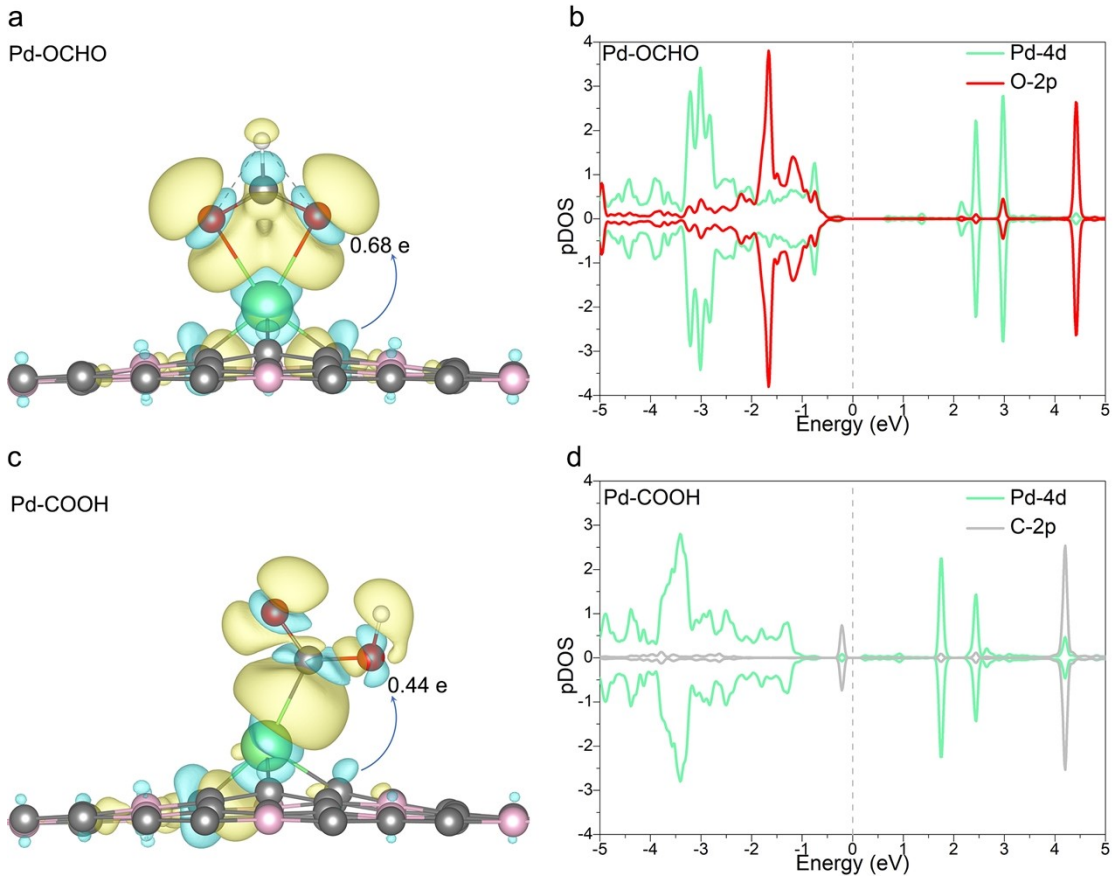

Figure S16. Electronic interpretation of HCOOH activity and selectivity on Pd@BC_3. (a) Charge density difference (CDD) between Pd@BC_3 and the adsorbed OCHO (Pd-OCHO). **(b)** Projected density of states (pDOS) of Pd-4d, O-2p and C-2p in the adsorption system (Pd-OCHO). The O-2p and C-2p states are derived from the *OCHO intermediate. **(c)** CDD between Pd@BC_3 and the *COOH intermediate (denoted by Pd-COOH). **(d)** pDOS of Pd-4d, O-2p and C-2p in the adsorption system (Pd-COOH). The O-2p and C-2p states are derived from the *COOH intermediate. Yellow and cyan regions indicate the accumulation and depletion of electron densities at the isosurface value of 0.002 e/$Å^3$.

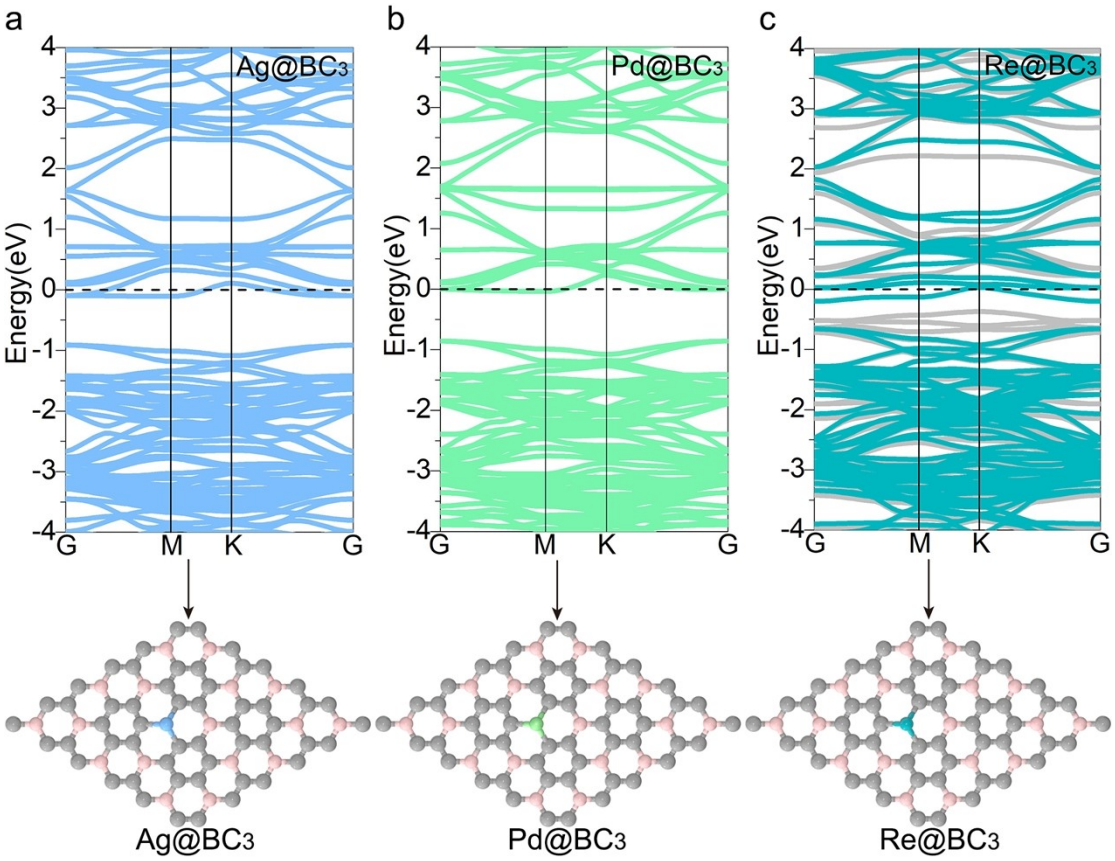

Figure S17. Band structures of **(a)** Ag@BC_3, **(b)** Pd@BC_3 and **(c)** Re@BC_3. The atomic structures are shown below. Re@BC_3 exhibits magnetism, and the band structures for both spin-up (grey) and spin-down (dark cyan) are plotted in the figure.

REFERENCES

(1) Nørskov, J. K.; Rossmeisl, J.; Logadottir, A.; Lindqvist, L.; Kitchin, J. R.; Bligaard, T.; Jónsson, H. Origin of the Overpotential for Oxygen Reduction at a Fuel-Cell Cathode. *The Journal of Physical Chemistry B* **2004**, *108*(46), 17886-17892, DOI: 10.1021/jp047349j.

(2) Xudong Cui, W. A.; Xiaoyang Liu, H. W.; Yong Men, J. W. C_2N-graphene supported single-atom catalysts for CO_2 electrochemical reduction reaction: mechanistic insight and catalyst screening. *Nanoscale* **2018**, *10*(32), 15262-15272, DOI: 10.1039/C8NR04961K.

(3) Ou, J.; Kang, X.; Duan, X. In silico design of single transition metal atom anchored defective boron carbide monolayers as high-performance electrocatalysts for the nitrogen reduction reaction. *Nanoscale* **2022**, *14*(32), 12823-12829, DOI: 10.1039/d2nr02796h.

(4) Wang, Y.; Zhou, N.; Li, Y. Electrochemical catalytic mechanism of single transition metal atom embedded BC_3 monolayer for oxygen reduction and evolution reactions. *Chem. Eng. J.* **2021**, *425*, 130631, DOI: 10.1016/j.cej.2021.130631.

(5) Yanagisawa, H.; Tanaka, T.; Ishida, Y.; Matsue, M.; Rokuta, E.; Otani, S.; Oshima, C. Phonon Dispersion Curves of a BC_3 Honeycomb Epitaxial Sheet. *Phys. Rev. Lett.* **2004**, *17*(93), 177003, DOI: 10.1103/PhysRevLett.93.177003.

(6) Liu, J.; Smith, S. C.; Gu, Y.; Kou, L. C—N Coupling Enabled by N—N Bond Breaking for Electrochemical Urea Production. *Adv. Funct. Mater.* **2023**, *33*(47), DOI: 10.1002/adfm.202305894.

(7) Xu, H.; Cheng, D.; Cao, D.; Zeng, X. C. Revisiting the universal principle for the rational design of single-atom electrocatalysts. *Nature Catalysis* **2024**, *7*(2), 207-218, DOI: 10.1038/s41929-023-01106-z.